Received 23 August 2021; accepted 6 September 2021. Date of publication 16 September 2021; date of current version 24 September 2021.

Digital Object Identifier 10.1109/OJCOMS.2021.3113023

Wireless-Powered Full-Duplex UAV Relay Networks Over FTR Channels

DANIEL DE PAIVA MUCIN [1], DIANA PAMELA MOYA OSORIO [2] (Member, IEEE), AND EDGAR EDUARDO BENITEZ OLIVO [1] (Member, IEEE)

[1]São Paulo State University (UNESP), Campus of São João da Boa Vista, São João da Boa Vista 13876-750, Brazil

[2]Centre for Wireless Communications, University of Oulu, 90014 Oulu, Finland

CORRESPONDING AUTHOR: D. P. M. Osorio (e-mail: diana.moyaosorio@oulu.fi)

This work was supported in part by the National Council for Scientific and Technological Development (CNPq) under Grant 421850/2018-3, and in part by the Academy of Finland through 6Genesis Flagship under Grant 318927 and FAITH Project under Grant 334280.

ABSTRACT A thorough understanding of fundamental limits of wireless-powered unmanned aerial vehicle (UAV) relay networks in millimeter waves is still missing. We narrow this gap by investigating the outage performance of a UAV-assisted wireless network over fluctuating two-ray (FTR) channels. The FTR fading model is particularly appealing since well characterizes the wireless propagation in a wide range of frequencies, including those in millimeter waves. The proposed setup consists of a source-destination pair communicating with the assistance of a UAV, which is a wireless-powered relay station operating in full-duplex mode under the amplify-and-forward protocol. For the wireless energy harvesting at the UAV, wireless power transfer (WPT), simultaneous wireless information and power transfer (SWIPT), and self-recycling energy techniques are employed together. To characterize the system outage probability, we obtain an integral-form expression derived from an approximate analysis and a simple closed-form expression derived from an asymptotic analysis at the high signal-to-noise ratio (SNR) regime. Monte Carlo simulations are provided to validate the correctness of our theoretical results and provide insights on the network performance in terms of key system parameters. Interestingly, obtained results show that the FTR fading parameters corresponding to the first hop and second hop play no role on the system outage performance at high SNR. Instead, it is mainly governed by the effect of the residual self-interference at the UAV, leading to outage floors.

INDEX TERMS Fluctuating two-ray, full duplex, mmWave communications, outage probability, simultaneous wireless information and power transfer, unmanned aerial vehicle.

I. INTRODUCTION

A. MOTIVATION AND BACKGROUND

RECENTLY, wireless communications based on unmanned aerial vehicles (UAVs) have received special attention from the scientific community, due to inherent characteristics of UAVs, such as: facility in performing maneuvers, ability to remain stable at precise altitudes, and low acquisition and maintenance costs. In the context of fifth generation (5G) and beyond-5G (B5G) wireless networks, which are devised to support ever increasing data rates, high reliability, very low latency and high energy efficiency [1], UAVs are expected to be introduced as relay stations to enable reliable communications in various use cases, including live video broadcasting, temporary radio access for connectivity in isolated areas, crowded scenarios, or even in disaster or emergency situations [2], [3].

As for cooperative techniques, two relaying protocols are widely known, namely: decode-and-forward (DF) [4], in which the relay decodes the information from the source and then re-encodes it before sending it to the destination; and amplify-and-forward (AF) [5], in which the relay merely amplifies the received signal from a source, with a fixed or variable gain, and then send it to the destination, thus requiring a lower implementation complexity when

compared to the DF protocol, while maintaining a comparable performance at medium-to-high signal-to-noise ratio (SNR). In addition, relay stations can operate in two relaying modes: half duplex (HD) and full duplex (FD). The FD mode provides improved spectral efficiency, since the relay is able to receive and retransmit the information from the source in the same time-frequency channel, thus recovering the penalty in spectral efficiency inherent to the HD mode, which requires non-overlapping time-frequency channels for the information transmission and reception [6]. However, the penalty in this case comes from the self-interference (SI) suffered at the receiver antenna of the relay from its own transmitter antenna, as a consequence of the simultaneous retransmission. In this regard, SI mitigation techniques have been the subject of several research efforts based on propagation, analog, and digital-domain approaches [7]–[9].

On the other hand, in order to enhance the overall energy efficiency in B5G networks, wireless power transfer (WPT) can be used to enable devices to gather energy from radio frequency (RF) signals [10]. Plus, simultaneous wireless information and power transfer (SWIPT) techniques have been proposed to provide a spectral efficiency gain in addition to the energy efficiency one, as in this case devices are able to divide the energy of the received RF signal into two parts: one for energy harvesting (EH) and one for information decoding (ID). In this respect, two techniques are commonly used: time switching (TS), whereby different time intervals are allocated for EH and another for ID [11]; and power splitting (PS), whereby the received RF signal is split into two flows with different power levels, one of which is sent to a rectifier circuit for EH and another is converted to a baseband signal for ID [12]. For EH purposes, linear and nonlinear EH models have been proposed. Nonlinear EH models consider a nonlinear function of the received RF signal due to the non-linearity of some EH circuit components (e.g., diodes) [13], [14]. This way, a nonlinear EH model is more realistic than the linear one, in which the harvested energy is linearly proportional to the received RF power. However, the linear EH model is shown to be suitable for certain input power range (cf. [13, Fig. 2]), in addition to render the mathematical analysis tractable.

The benefits of FD systems with WPT were assessed in [15], [16], and those of FD systems with SWIPT were assessed in [17]. For instance, in [15], the authors provided an analytical characterization of the achievable throughput of three different communication modes in a dual-hop FD relaying system, where the energy constrained relay node is powered by RF signals from the source using the TS architecture. Therein, both AF and DF relaying protocols were considered. In [16], the instantaneous throughput of a FD-DF system with WPT was maximized by optimizing the receive and transmit beamformers at a multi-antenna relay and the time-splitting factor. On the other hand, in [17], the authors proposed a beam-domain hybrid TS- and PS-based SWIPT scheme for a FD massive multiple-input multiple-output (MIMO) system. More specifically, therein it was considered a FD base station serving a set of HD users.

In light of this, UAV-assisted wireless networks using SWIPT have received special attention from the scientific community, as the combined use of cooperative communications and SWIPT techniques can simultaneously improve the reliability, spectral efficiency, and energy efficiency of the system (see, for example, [21], [22], [25]).

Moreover, in order to achieve higher data rates and meet the requirements of high volumes of data traffic, communication in the millimeter wave (mmWave) band is a key enabler for this purpose, due to the large bandwidth available at this part of the radio frequency spectrum. However, as a downside, signals in the mmWave range are more sensitive to the propagation attenuation and obstacle blockage. In this sense, mmWave communications can be aided by UAVs operating at a certain height in order to extend the transmission range and even provide a line-of-sight (LOS) link between transmitter and receiver [18]. In this context, the fluctuating two-ray (FTR) fading model, recently proposed in [19], has been shown to provide a much better fit to field measurements for outdoor mmWave communications, when compared to the Rayleigh and Rician fading models [19], [20]. In fact, the FTR fading model is a generalized statistical channel model which includes the Rayleigh, Rician, Nakagami-*m*, Hoyt, and Rician shadowed distributions as particular cases, among others (cf. [19, Table I]). This way, the FTR fading model allows to characterize a wide heterogeneity of fading scenarios with and without LOS, thereby being a suitable, versatile model for UAV-assisted communications operating in the mmWave frequency range [21].

B. RELATED WORKS

As for UAV-assisted wireless networks, in [22], a performance analysis in terms of the outage probability of a HD UAV-assisted cooperative network with a FD ground station was performed for Rician shadowed fading channels. However, in that work, the use of SWIPT techniques was not considered.[1] Recently, in [21], the outage probability of a UAV-assisted cooperative network operating under the AF and DF relaying protocols with SWIPT was analyzed over FTR fading channels. In [23], the outage performance of a HD-AF UAV-based relaying network with EH in urban environment was assessed. In that work, Rician shadowed fading and Rayleigh shadowed fading were considered to characterize the LOS and non-line-of-sight (NLOS) propagation scenarios, respectively. In [24], the end-to-end cooperative throughput maximization problem was studied for a

1. It is worthwhile to mention that the Rician shadowed fading model is one of the particular cases of the FTR fading model. In fact, both fading models account for any amplitude fluctuation in the specular components—a single specular component in the case of the Rician shadowed fading model and two specular components in the case of the FTR fading model—, as a result of fast moving scatterers or electromagnetic disturbances in the propagation condition [19].

HD UAV-assisted cooperative communication system with SWIPT, in which the UAV was powered by RF signals coming from the source and both AF and DF relaying protocols were considered. Nonetheless, in [21], [23], [24], only the HD relaying mode was considered; consequently, the system spectral efficiency was halved when compared to the FD relaying mode.

In [25], the performance of a FD UAV-assisted cooperative network operating under the DF protocol with SWIPT was evaluated in terms of the outage probability over Rayleigh fading channels. Therein, a WPT-based relaying strategy was proposed, in which initially a time interval is allocated for wireless powering the UAV from the source in order to improve the battery life and, consequently, its flight time, and, in a second time interval, the UAV performs SWIPT with EH from the residual SI link.

In [26], the performance of a HD UAV-assisted cognitive radio network with underlay spectrum sharing operating under the DF protocol with EH was analyzed in terms of the secrecy outage probability over Nakagami-*m* fading channels. Recently, in [27], the exact closed-form expressions for the outage probability and throughput were derived for a wireless localization system based on EH, aided by a HD-DF UAV, over Nakagami-*m* fading and lognormal shadowing to take into account small- and large-scale effects. However, in both [26], [27], only the HD relaying mode was considered, while SWIPT techniques were not employed, thus diminishing the overall network spectral efficiency when compared to joint use of FD- and SWIPT-based approaches. More recently, in [28], [29], the use of a FD-UAV relay in wireless networks was investigated. In [28], the authors formulated a problem for maximization of the achievable rate from a source to the destination nodes with the cooperation of a FD-UAV. In [29], a joint optimization problem to maximize the system throughput of a FD-UAV-assisted network with multiple source-destination pairs was formulated. However, in both [28], [29], SWIPT techniques were not considered, thus also attaining reduced overall network spectral efficiency with respect to a strategy that exploits both FD and SWIPT.

C. PROPOSAL AND CONTRIBUTIONS

Despite the remarkable contributions so far, a thorough understanding of fundamental limits of wireless-powered UAV relay networks over mmWave channels is still open for investigation. This paper aims to contribute in this context. In particular, we investigate a network setup consisting of a source which communicates with a destination, aided by a wireless-powered UAV. In this setup, the UAV is considered to operate in FD relaying mode and under the AF protocol. The FTR channel model is considered to characterize the effects of fading in the mmWave frequency range. Motivated by [25], in order to improve the spectral efficiency and energy efficiency of the system, each transmission block is assumed to be made up of two consecutive phases: (*i*) a WPT phase to power the UAV through RF signals coming from the source and (*ii*) a PS-based SWIPT phase to enable the UAV to simultaneously harvest energy and decode information from the source's signal, as well as self-recycling energy from the self-interference at the UAV inherent to the FD operation mode. To the best of the authors' knowledge, there is no literature addressing the study of FD UAV-assisted wireless networks operating under the AF protocol with SWIPT over FTR channels.[2] The following are our main contributions:

- An analytical expression for the end-to-end instantaneous received signal-to-interference-plus-noise ratio (SINR) is obtained.
- An integral-form expression for the approximate outage probability of the considered system is derived, the accuracy of which is verified by numerical simulations for different illustrative cases. It is worthwhile to mention that the underlying problem proves rather involved in view of the system model complexity, as shall be detailed later.
- To reduce the computational complexity of the previously-mentioned approximate analytical result, a simple, compact, closed-form expression for the outage probability is derived from an asymptotic analysis at high SNR.
- The impact of key system parameters on the outage performance is investigated, including the time allocation factor between the WPT and SWIPT phases, the average channel gain of the self-interference link, and the FTR fading model parameters.

The remainder of this paper is outlined as follows. Section II introduces the system model. Section III characterizes the signal model, from which the end-to-end SINR for the considered system is obtained. Then, the outage probability is investigated in Section IV by performing approximate and asymptotic analyses. Section V illustrates numerical results for sample scenarios which validate the foregoing analyses. Finally, Section VI concludes this work.

Notation: Throughout this paper, we use $f_X(\cdot)$ and $F_X(\cdot)$ to denote the probability density function (PDF) and cumulative distribution function (CDF) of a random variable X, respectively, $E[\cdot]$ to denote expectation, $\Pr[\cdot]$ to denote probability, and "$\simeq$" to denote asymptotic equivalence.

II. SYSTEM MODEL

Consider a UAV-assisted wireless network as illustrated in Fig. 1, consisting of a source (S) and a destination (D) as ground nodes and a FD-AF UAV acting as a relay (R), which is hovering at certain altitude to assist in the communication between S and D.[3] The direct link S→D is assumed to be severely attenuated due to the presence of obstacles and, therefore, the communication between S and D is possible

2. As previously mentioned, recall that [25] addressed a FD UAV-assisted network based on the DF protocol over Rayleigh fading.

3. It is considered that the UAV's position remains unchanged (or that the UAV's speed is sufficiently low) during a certain time interval after a positioning process is accomplished in order to serve the ground users [30].

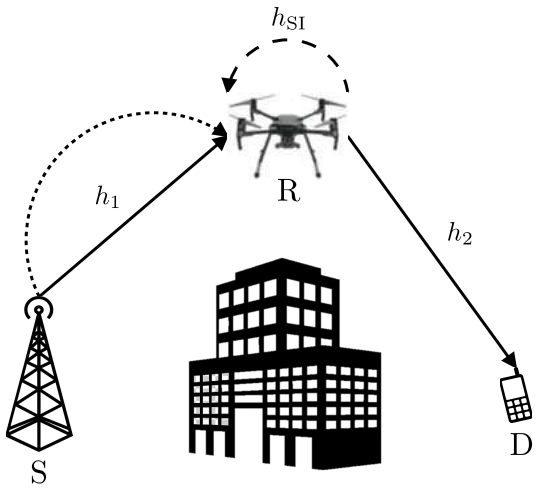

FIGURE 1. System model (information transmission: solid line; energy transfer: dotted line; interference signal: dashed line).

only through the relaying link enabled by R. All nodes in the network are considered to have a single antenna, except for the UAV, which is equipped with two antennas (one for transmission and one for reception), in order to enable the FD relaying mode. Let us denote h_1 and h_2 as the channel coefficients of the links S→R (ground base station-UAV or first hop) and R→D (UAV-destination or second hop), respectively, which are assumed to be subject to independent and non-identically (i.n.i.d.) distributed FTR fading, and h_{SI} as the channel coefficient of the residual SI link at the UAV operating in FD relaying mode. In this respect, it is worthwhile to mention that even though the LOS component between the transmitting and receiving antennas at the UAV can be strongly attenuated after (passive/active) SI cancellation stages, there remains a residual SI due to imperfections in the cancellation process, so that the residual SI link is assumed to undergo Rayleigh fading [7], [8]. Moreover, all nodes are considered to experience additive white Gaussian noise (AWGN) with average power N_0 at their receivers. Further details and background concepts on the system model are provided in the next subsections.

A. FTR FADING CHANNEL

For completeness, here we revisit some background concepts regarding the FTR fading model. According to the this model, the complex channel coefficient h_i, $i \in \{1, 2\}$, is composed of two specular components with amplitudes $V_{i,1}$ and $V_{i,2}$ and random phases $\phi_{i,1}$ and $\phi_{i,2}$, respectively, plus a diffuse component which characterizes the multipath propagation, that is [19]

$$h_i = \sqrt{\zeta_i} V_{i,1} \exp\left(j\phi_{i,1}\right) + \sqrt{\zeta_i} V_{i,2} \exp\left(j\phi_{i,2}\right) + X_i + jY_i, \quad (1)$$

where ζ_i is a Gamma distributed random variable with unit mean and parameter m_i [19, eq. (3)], which characterizes the fluctuations of the specular components—these fluctuations can be more or less pronounced as the value of m_i decreases or increases, respectively—; $\phi_{i,1}$ and $\phi_{i,2}$ are uniformly distributed random phases, i.e., $\phi_{i,1}, \phi_{i,2} \sim \mathcal{U}[0, 2\pi)$; and $X_i + jY_i$ is the diffuse component, with X_i and Y_i being Gaussian random variables with zero mean and variance ${\sigma_i}^2$, i.e., $X_i, Y_i \sim \mathcal{N}(0, {\sigma_i}^2)$. The FTR model depends on the following parameters:

$$K_i = \frac{\left(V_{i,1}^2 + V_{i,2}^2\right)}{2{\sigma_i}^2}, \quad (2)$$

$$\Delta_i = \frac{2V_{i,1}V_{i,2}}{\left(V_{i,1}^2 + V_{i,2}^2\right)}, \quad (3)$$

where K_i is the ratio of the average power of the specular components to the power of the diffuse multipath component, and $0 \leq \Delta_i \leq 1$ stands for the similarity between the specular components in terms of their average powers, such that the average powers of these components are equal for $\Delta_i = 1$, and one of the two components is nil for $\Delta_i = 0$. Besides, the average channel gain for the FTR model is given by

$$\Omega_i = E\{g_i\} = 2{\sigma_i}^2(1 + K_i), \quad (4)$$

where $g_i = |h_i|^2$ is the corresponding channel gain.

The PDF and CDF of a channel gain undergoing FTR fading are given, respectively, by [31, eqs. (18) and (19)]

$$f_{g_i}(x) = \frac{\left(\frac{m_i}{K_i}\right)^{m_i}}{\Gamma(m_i)} \sum_{j=0}^{\infty} \frac{\tau_j(K_i, \Delta_i, m_i)}{j!} \frac{x^j \exp\left(-\frac{x}{2{\sigma_i}^2(\Omega_i, K_i)}\right)}{\Gamma(j+1)\left(2{\sigma_i}^2(\Omega_i, K_i)\right)^{j+1}}, \quad (5)$$

$$F_{g_i}(x) = \frac{\left(\frac{m_i}{K_i}\right)^{m_i}}{\Gamma(m_i)} \sum_{j=0}^{\infty} \frac{\tau_j(K_i, \Delta_i, m_i)}{j!\Gamma(j+1)} \gamma\left(j+1, \frac{x}{2{\sigma_i}^2(\Omega_i, K_i)}\right), \quad (6)$$

where $\gamma(\cdot, \cdot)$ is the incomplete gamma function [32, eq. (8.350.1)], and

$$\tau_j(K_i, \Delta_i, m_i) = \sum_{k=0}^{j} \binom{j}{k} \sum_{l=0}^{k} \binom{k}{l} \sum_{n=0}^{w} (-1)^{2n+2l-k} \left(\frac{\Delta_i}{2}\right)^{2n+2l} \times \chi(n, w, 2l-k)\Gamma(\lambda)\left(1 + \frac{m_i}{K_i}\right)^{-\lambda}, \quad (7)$$

with $\chi(n, w, 2l-k) = \frac{\Gamma(w+n)}{\Gamma(n+1)\Gamma(w-n+1)} \frac{w^{1-2n}}{\Gamma(2l-k+n+1)}$ and $\lambda = j + 2l - k + 2n + m_i$.

Remark 1: It is noteworthy that the FTR fading model was first introduced in [19], along with a detailed statistical characterization of the corresponding PDF and CDF expressions. By virtue of the versatility and suitability of this model for mmWave scenarios, some works have addressed their efforts in proposing simplified expressions for the PDF and CDF [31], [33]–[35]. In particular, the authors in [35] provided new exact analytical expressions for the PDF and CDF of the FTR fading model. However, those expressions were provided in terms of special functions, more specifically, the Legendre functions of the first kind [32, eq. (8.702)], which are not a built-in functions in most standard computing software, such as MATLAB. Alternatively, the authors in [31] derived exact analytical expressions for the PDF and CDF of a product of N independent FTR random variables, including the case $N = 1$ (for a single hop). Conveniently,

TABLE 1. Empirical parameters for LOS probability scenarios.

	a	b	c	d	e
Suburban	101.6	0	0	3.25	1.241
Urban	120.0	0	0	24.30	1.229
Dense Urban	187.3	0	0	82.10	1.478
Urban High-Rise	352.0	-1.37	-53	173.80	4.670

the expressions in that work, revisited here in (5) and (6), were attained in terms of elementary functions. We will use these expressions in our analysis.

As mentioned above, the S→R and R→D links are considered to undergo i.n.i.d. FTR fading, characterized by the distribution functions given in (5) and (6), while the residual SI link is considered to undergo Rayleigh fading—this latter being a particular case of the FTR fading model, for $\Delta_i = 0$ and $K_i = 0$ [19]. Thus, the PDF and CDF of the channel gain g_{SI} at the residual SI link are given as

$$f_{g_{\mathrm{SI}}}(x) = \frac{1}{\Omega_{\mathrm{SI}}} \exp\left(-\frac{x}{\Omega_{\mathrm{SI}}}\right), \tag{8}$$

$$F_{g_{\mathrm{SI}}}(x) = 1 - \exp\left(-\frac{x}{\Omega_{\mathrm{SI}}}\right). \tag{9}$$

B. UAV ALTITUDE PARAMETERS AND LOS PROBABILITY

Let us consider that S, R and D are located in a three-dimensional topology, the coordinates of which are $(\mathrm{S}_x, \mathrm{S}_y, \mathrm{S}_z)$, $(\mathrm{R}_x, h, \mathrm{R}_z)$, and $(\mathrm{D}_x, \mathrm{D}_y, \mathrm{D}_z)$, respectively, with h being the UAV flight height from the ground. The distance between the UAV and the ground nodes is given by the Euclidean distance and the elevation angle of the UAV with respect to a ground node can be obtained as

$$\theta = \tan^{-1}\left(\frac{h}{\mathrm{R}_x}\right). \tag{10}$$

The probability of LOS propagation between the UAV and a ground node can be approximated as [36]

$$P_{\mathrm{LOS}} \approx a - \frac{a-b}{1 + \left(\frac{\theta - c}{d}\right)^e}, \tag{11}$$

where a, b, c, d, and e are empirical parameters for four typical environments: (*i*) suburban; (*ii*) urban; (*iii*) dense urban; and (*iv*) urban high-rise, the values of which are given in Table 1 [36]. Consequently, the probability of NLOS propagation is given by

$$P_{\mathrm{NLOS}} = 1 - P_{\mathrm{LOS}}. \tag{12}$$

C. ENERGY TRANSFER AND INFORMATION TRANSMISSION SCHEME

With the aim of saving battery's energy at the UAV to provide communications, it is considered that the UAV's wireless transmission capability is powered from the energy harvested from the RF signals coming from both S and the SI link, while the UAV's maneuvering is powered by a separated on-board battery [24]. Assuming a time division multiple access

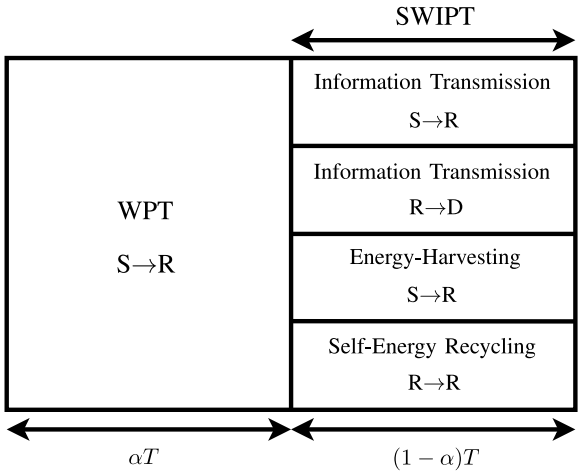

FIGURE 2. Transmission scheme, where α denotes the time allocation factor between the WPT and SWIPT phases.

scheme, it is considered that each communication process occurs in a time interval of duration T, which is composed of two phases with duration determined by a time allocation factor $\alpha \in (0, 1)$, as illustrated in Fig. 2: (*i*) WPT phase, in which R is energized by RF signals coming from S during a time subinterval αT, with total available transmit power at S, P_{S}; and (*ii*) SWIPT phase, in which the PS technique is used for simultaneous information and power transfer from S to R, while R forwards information to D (since the UAV operates in FD mode) and self-recycles energy from the SI link, all of this occurring during a time subinterval $\bar{\alpha}T$, where $\bar{\alpha} = 1 - \alpha$. In this latter phase, a portion ρ of the received power at R is used for ID, where $\rho \in (0, 1)$ is the power splitting factor relative to SWIPT, while a portion $\bar{\rho} = 1 - \rho$ of the total received power at R coming from the signals of S and the SI link is used for EH and self-energy recycling, respectively. Meanwhile, the total available transmit power at R, P_{R}, is used for relaying information to D.

Considering this, the energy transferred to the UAV during the WPT phase is given by

$$E_{\mathrm{WPT}} = \eta \alpha T P_{\mathrm{S}} g_1, \tag{13}$$

where $\eta \in (0, 1]$ is the energy conversion efficiency factor, whereas in the SWIPT phase, the energy harvested at the UAV from S and the SI link is given by

$$E_{\mathrm{SWIPT}} = \eta \bar{\rho} \bar{\alpha} T (P_{\mathrm{S}} g_1 + P_{\mathrm{R}} g_{\mathrm{SI}}), \tag{14}$$

where P_{R} is given by the ratio between the total energy harvested during the WPT and SWIPT phases and the duration of information transmission, that is

$$P_{\mathrm{R}} = \frac{E_{\mathrm{WPT}} + E_{\mathrm{SWIPT}}}{\bar{\alpha} T} = \frac{\eta P_{\mathrm{S}} g_1}{1 - \eta \bar{\rho} g_{\mathrm{SI}}} \left(\frac{\alpha}{\bar{\alpha}} + \bar{\rho}\right). \tag{15}$$

III. SIGNAL ANALYSIS

Based on the system model introduced in Section II, in this section a signal analysis is developed in order to determine

the end-to-end instantaneous received SINR. We have that the received information signal at the UAV during the SWIPT phase (in the interval $\bar{\alpha}T$) is given by

$$y_{\mathrm{R}}(t) = h_1\sqrt{\rho P_{\mathrm{S}}}x_{\mathrm{S}}(t) + h_{\mathrm{SI}}\sqrt{\rho P_{\mathrm{R}}}x_{\mathrm{R}}(t) + n_{\mathrm{R}}(t), \quad (16)$$

where $x_{\mathrm{S}}(t)$ is the information signal transmitted by S; $x_{\mathrm{R}}(t) = \mathcal{G}y_{\mathrm{R}}(t - T_a)$ is the signal retransmitted by R, with $\mathcal{G}$ being the amplification factor relative to the AF protocol and T_a being the processing delay inherent to the FD relaying mode, so that the received and retransmitted signals at R are uncorrelated [37]; and $n_{\mathrm{R}}(t)$ is noise component at R. Using (16) in the definition of $x_{\mathrm{R}}(t)$, by means of recursive substitutions, it can be rewritten as

$$\begin{aligned} x_{\mathrm{R}}(t) &= \mathcal{G}\sum_{j=1}^{N}\left(h_{\mathrm{SI}}\sqrt{\rho P_{\mathrm{R}}}\mathcal{G}\right)^{j-1}\Big[h_1\sqrt{\rho P_{\mathrm{S}}}x_{\mathrm{S}}(t - jT_a) \\ &\qquad + n_{\mathrm{R}}(t - jT_a)\Big] \\ &= \mathcal{G}h_1\sqrt{\rho P_{\mathrm{S}}}x_{\mathrm{S}}(t - T_a) \\ &\quad + \mathcal{G}\sum_{j=2}^{N}\left(h_{\mathrm{SI}}\sqrt{\rho P_{\mathrm{R}}}\mathcal{G}\right)^{j-1}\Big[h_1\sqrt{\rho P_{\mathrm{S}}}x_{\mathrm{S}}(t - jT_a) \\ &\qquad + n_{\mathrm{R}}(t - jT_a)\Big] \\ &\quad + \mathcal{G}n_{\mathrm{R}}(t - T_a). \end{aligned} \quad (17)$$

By assuming normalized unit-power signals, that is $E\{|x_{\mathrm{S}}(t)|^2\} = E\{|x_{\mathrm{R}}(t)|^2\} = 1$, it follows from (17) that

$$E\left\{|x_{\mathrm{R}}(t)|^2\right\} = \mathcal{G}^2\sum_{j=1}^{N}\left(g_{\mathrm{SI}}\rho P_{\mathrm{R}}\mathcal{G}^2\right)^{j-1}\left[g_1\rho P_{\mathrm{S}} + N_0\right], \quad (18)$$

where $N_0 = E\{|n_{\mathrm{R}}(t)|^2\}$ is the average noise power. Then, for $\mathcal{G}^2 < [g_{\mathrm{SI}}\rho P_{\mathrm{R}}]^{-1}$, the geometric series in (18) is convergent, so that, by considering $E\{|x_{\mathrm{R}}(t)|^2\} = 1$, the amplification factor can be obtained as

$$\mathcal{G} = \sqrt{\frac{1}{g_1\rho P_{\mathrm{S}} + g_{\mathrm{SI}}\rho P_{\mathrm{R}} + N_0}}. \quad (19)$$

On the other hand, the received information signal at D is given by

$$y_{\mathrm{D}}(t) = h_2\sqrt{P_{\mathrm{R}}}x_{\mathrm{R}}(t) + n_{\mathrm{D}}(t), \quad (20)$$

where $n_{\mathrm{D}}(t)$ is the noise component at D, with average power $E\{|n_{\mathrm{D}}(t)|^2\} = N_0$.

By replacing (17) into (20), the received power at D can be obtained as

$$\begin{aligned} E\left\{|y_{\mathrm{D}}(t)|^2\right\} &= \underbrace{\mathcal{G}^2\rho P_{\mathrm{S}}g_1P_{\mathrm{R}}g_2}_{\text{Signal of interest}} \\ &\quad + \underbrace{\frac{\mathcal{G}^4\rho P_{\mathrm{R}}^2g_2g_{\mathrm{SI}}(\rho P_{\mathrm{S}}g_1 + N_0)}{1 - g_{\mathrm{SI}}\rho P_{\mathrm{R}}\mathcal{G}^2}}_{\text{Self-interference signal}} \\ &\quad + \underbrace{N_0\left(\mathcal{G}^2P_{\mathrm{R}}g_2 + 1\right)}_{\text{Noise signal}}. \end{aligned} \quad (21)$$

Then, the instantaneous received end-to-end SINR, γ_{e2e}, can be attained from (21) as

$$\gamma_{\mathrm{e2e}} = \frac{\mathcal{G}^2\rho P_{\mathrm{S}}g_1P_{\mathrm{R}}g_2}{\frac{\mathcal{G}^4\rho P_{\mathrm{R}}^2g_2g_{\mathrm{SI}}(\rho P_{\mathrm{S}}g_1 + N_0)}{1 - g_{\mathrm{SI}}\rho P_{\mathrm{R}}\mathcal{G}^2} + \left(\mathcal{G}^2P_{\mathrm{R}}g_2 + 1\right)N_0}. \quad (22)$$

By substituting (15) and (19) into (22) and dividing the resulting expression by N_0^2, we obtain

$$\gamma_{\mathrm{e2e}} = \frac{\frac{\rho\gamma_{\mathrm{S}}g_1}{\frac{\rho\eta\gamma_{\mathrm{S}}g_1g_{\mathrm{SI}}}{1 - \eta\bar{\rho}g_{\mathrm{SI}}}\left(\frac{\alpha}{\bar{\alpha}} + \bar{\rho}\right) + 1}\frac{\eta\gamma_{\mathrm{S}}g_1g_2}{1 - \eta\bar{\rho}g_{\mathrm{SI}}}\left(\frac{\alpha}{\bar{\alpha}} + \bar{\rho}\right)}{\frac{\rho\gamma_{\mathrm{S}}g_1}{\frac{\rho\eta\gamma_{\mathrm{S}}g_1g_{\mathrm{SI}}}{1 - \eta\bar{\rho}g_{\mathrm{SI}}}\left(\frac{\alpha}{\bar{\alpha}} + \bar{\rho}\right) + 1} + \frac{\eta\gamma_{\mathrm{S}}g_1g_2}{1 - \eta\bar{\rho}g_{\mathrm{SI}}}\left(\frac{\alpha}{\bar{\alpha}} + \bar{\rho}\right) + 1}, \quad (23)$$

where $\gamma_{\mathrm{S}} = P_{\mathrm{S}}/N_0$ is the transmit SNR at the source. Now let us define

$$\beta(g_1, g_{\mathrm{SI}}) \triangleq \frac{\eta\gamma_{\mathrm{S}}g_1}{1 - \eta\bar{\rho}g_{\mathrm{SI}}}\left(\frac{\alpha}{\bar{\alpha}} + \bar{\rho}\right), \quad (24)$$

so that

$$X \triangleq \rho\gamma_{\mathrm{S}}g_1, \quad (25)$$

$$Y \triangleq \beta(g_1, g_{\mathrm{SI}})g_2, \quad (26)$$

$$U \triangleq \rho\beta(g_1, g_{\mathrm{SI}})g_{\mathrm{SI}}, \quad (27)$$

stand for the instantaneous received SNR at the first hop, second hop, and SI link, respectively. Thus. the instantaneous received end-to-end SINR in (23) can be rewritten as

$$\gamma_{e2e} = \frac{\frac{XY}{U+1}}{\frac{X}{U+1} + Y + 1}. \quad (28)$$

Next we perform an outage analysis for the system under study based on this latter expression.

IV. OUTAGE ANALYSIS

For the considered wireless-powered FD UAV relay system undergoing FTR fading, the overall outage probability can be formulated as

$$\begin{aligned} P_{\mathrm{out}} &= P_{1,\mathrm{LOS}}P_{2,\mathrm{LOS}}P_{\mathrm{out}}^{\mathrm{e2e}}\big(K_{1,\mathrm{LOS}}, \Delta_{1,\mathrm{LOS}}, m_{1,\mathrm{LOS}}, \\ &\qquad K_{2,\mathrm{LOS}}, \Delta_{2,\mathrm{LOS}}, m_{2,\mathrm{LOS}}\big) \\ &\quad + P_{1,\mathrm{LOS}}P_{2,\mathrm{NLOS}}P_{\mathrm{out}}^{\mathrm{e2e}}\big(K_{1,\mathrm{LOS}}, \Delta_{1,\mathrm{LOS}}, m_{1,\mathrm{LOS}}, \\ &\qquad K_{2,\mathrm{NLOS}}, \Delta_{2,\mathrm{NLOS}}, m_{2,\mathrm{NLOS}}\big) \\ &\quad + P_{1,\mathrm{NLOS}}P_{2,\mathrm{LOS}}P_{\mathrm{out}}^{\mathrm{e2e}}\big(K_{1,\mathrm{NLOS}}, \Delta_{1,\mathrm{NLOS}}, m_{1,\mathrm{NLOS}}, \\ &\qquad K_{2,\mathrm{LOS}}, \Delta_{2,\mathrm{LOS}}, m_{2,\mathrm{LOS}}\big) \\ &\quad + P_{1,\mathrm{NLOS}}P_{2,\mathrm{NLOS}}P_{\mathrm{out}}^{\mathrm{e2e}}\big(K_{1,\mathrm{NLOS}}, \Delta_{1,\mathrm{NLOS}}, m_{1,\mathrm{NLOS}}, \\ &\qquad K_{2,\mathrm{NLOS}}, \Delta_{2,\mathrm{NLOS}}, m_{2,\mathrm{NLOS}}\big), \end{aligned} \quad (29)$$

where the subscripts 1 and 2 are used to refer to the first hop (S→R link) and second hop (R→D link), respectively; $P_{i,\mathrm{LOS}}$ and $P_{i,\mathrm{NLOS}}$ are the probabilities of LOS and NLOS propagation at the ith hop, $i \in \{1, 2\}$, given by (11) and (12); $K_{i,\mathrm{LOS}}$, $\Delta_{i,\mathrm{LOS}}$, $m_{i,\mathrm{LOS}}$ and $K_{i,\mathrm{NLOS}}$, $\Delta_{i,\mathrm{NLOS}}$, $m_{i,\mathrm{NLOS}}$ are the fading parameters of the FTR distribution function in (5), which are set according to a LOS and NLOS propagation condition at the ith hop, respectively; and $P_{\mathrm{out}}^{\mathrm{e2e}}(\cdot, \ldots, \cdot) =$

$\Pr(\gamma_{\mathrm{e2e}} < \gamma_{\mathrm{th}})$ is the outage probability for the dual-hop FD UAV relay system under consideration, with the instantaneous received end-to-end SINR γ_{e2e} being given in (28) and γ_{th} being an outage SNR threshold.

Remark 2: Note that the four terms in the overall outage probability in (29) consider each of the propagation possibilities from a LOS or NLOS condition at the first hop and second hop. In this context, it is worthwhile to recall that the FTR fading model takes into account a wide range of fading scenarios, including LOS and NLOS propagation conditions. Accordingly, the three FTR fading parameters $(K_i,\ \Delta_i,\ m_i)$ in the outage probability $P_{\mathrm{out}}^{\mathrm{e2e}}(\cdot,\ldots,\cdot)$, corresponding to the ith hop, $i \in \{1, 2\}$, can be set to a given LOS or NLOS propagation condition.

We now focus our attention in the analysis of the outage probability $P_{\mathrm{out}}^{\mathrm{e2e}}(\cdot,\ldots,\cdot)$. In light of the complexity of the system under study, an exact analysis of $P_{\mathrm{out}}^{\mathrm{e2e}}(\cdot,\ldots,\cdot)$ proved rather intricate. Thus, in Section IV-A, we derive an integral-form approximation for the outage probability, which, importantly, shows to be highly accurate with respect to the exact system performance at the whole range of SNR values. Additionally, aiming at achieving useful insights on the system performance, in Section IV-B, we perform an asymptotic analysis of the outage probability, from which a simple closed-form expression is provided.

A. APPROXIMATE ANALYSIS

An approximation for the outage probability is obtained in the following proposition. As shall be seen in Section V, this approximation characterizes the exact system performance with high accuracy.

Proposition 1: An approximate analytical expression for the outage probability of a dual-hop wireless-powered FD UAV relay network over FTR channels is given by (30), shown at the bottom of the page, where

$$B = \frac{\bar{\alpha}\gamma_{\mathrm{th}}\bar{\rho}}{\gamma_{\mathrm{S}}\rho(\alpha + \gamma_{\mathrm{th}} - \bar{\alpha}\rho(1+\gamma_{\mathrm{th}}))}, \tag{31}$$

$$C(g_1) = \frac{-\bar{\alpha}(\gamma_{\mathrm{th}} - g_1\gamma_{\mathrm{S}}\rho)}{\eta\big(g_1\bar{\alpha}\bar{\rho}\rho\gamma_{\mathrm{S}} + \gamma_{\mathrm{th}}\big(-\bar{\alpha} + \rho - \alpha\rho + g_1\gamma_{\mathrm{S}}\rho + g_1\gamma_{\mathrm{S}}\rho^2\bar{\alpha}\big)\big)}, \tag{32}$$

$$D(g_1) = \frac{\gamma_{\mathrm{th}}\bar{\alpha}}{g_1\gamma_{\mathrm{S}}\eta(\bar{\rho} + \alpha\rho)}, \tag{33}$$

$$E(g_1, g_2) = \frac{\gamma_{\mathrm{th}}\bar{\alpha} + g_1 g_2 \eta\gamma_{\mathrm{S}}(-\bar{\rho} - \alpha\rho)}{\bar{\alpha}\bar{\rho}\eta\gamma_{\mathrm{th}}}. \tag{34}$$

Proof: See Appendix A. ■

B. ASYMPTOTIC ANALYSIS

In order to gain better insights into the impact of each system parameter on the communication performance, herein we develop a high-SNR outage analysis from which a closed-form expression is attained as in the following proposition.

Proposition 2: A closed-form asymptotic analytical expression for the outage probability of a dual-hop wireless-powered FD UAV relay network over FTR channels is given by

$$\begin{aligned} P_{\mathrm{out}}^{\mathrm{e2e}} \simeq\ & \exp\left(-\frac{\bar{\alpha}}{\Omega_{\mathrm{SI}}\eta(\bar{\alpha} + \gamma_{\mathrm{th}} - \bar{\alpha}\rho(1+\gamma_{\mathrm{th}}))}\right) \\ & - \exp\left(-\frac{2\bar{\alpha} + \gamma_{\mathrm{th}} - \bar{\alpha}\rho(2+\gamma_{\mathrm{th}})}{\Omega_{\mathrm{SI}}\eta\bar{\rho}(\bar{\alpha} + \gamma_{\mathrm{th}} - \bar{\alpha}\rho(1+\gamma_{\mathrm{th}}))}\right) \\ & + \exp\left(-\frac{2}{\Omega_{\mathrm{SI}}\eta\bar{\rho}}\right). \end{aligned} \tag{35}$$

Proof: See Appendix B. ■

Remark 3: Note from (35) that the asymptotic outage probability only depends on the following system parameters: (i) time allocation factor α between the WPT and SWIPT phases, (ii) power splitting factor ρ relative to the SWIPT phase; (iii) energy conversion efficiency factor η; (iv) outage SNR threshold γ_{th}; and (v) average channel gain Ω_{SI} at the residual SI link. Interestingly, note also that the FTR fading parameters corresponding to the first hop and second hop play no role on the high-SNR outage performance. In fact, we can notice that the expression in (35) characterizes an outage floor, as it does not depend on the transmit SNR. As shall be shown in the next section, the average

$$\begin{aligned} & P_{\mathrm{out}}^{\mathrm{e2e}}(K_1, \Delta_1, m_1, K_2, \Delta_2, m_2) \\ & \approx \frac{\left(\frac{m_1}{K_1}\right)^{m_1}}{\Gamma(m_1)} \sum_{j=0}^{\infty} \frac{\tau_j(K_1, \Delta_1, m_1)}{j!\Gamma(j+1)} \Bigg\{ \left[1 - \exp\left(-\frac{1}{\Omega_{\mathrm{SI}}\eta\bar{\rho}}\right)\right]\Gamma(j+1) + \frac{1}{\left[2{\sigma_1}^2(\Omega_1, K_1)\right]^{j+1}} \Bigg[\int_0^B v^j \exp\left(-\left(\frac{C(v)}{\Omega_{\mathrm{SI}}} + \frac{v}{2{\sigma_1}^2(\Omega_1, K_1)}\right)\right) dv \\ & - \int_{\frac{\gamma_{\mathrm{th}}}{\gamma_{\mathrm{S}}\rho}}^{\infty} \left(1 - \exp\left(-\frac{C(v)}{\Omega_{\mathrm{SI}}}\right)\right) v^j \exp\left(-\frac{v}{2{\sigma_1}^2(\Omega_1, K_1)}\right) dv \Bigg] + \frac{\left(\frac{m_2}{K_2}\right)^{m_2}}{\Gamma(m_2)} \sum_{i=0}^{\infty} \frac{\tau_i(K_2, \Delta_2, m_2)}{i!\Gamma(i+1)\left[2{\sigma_1}^2(\Omega_1, K_1)\right]^{j+1}\left[2{\sigma_2}^2(\Omega_2, K_2)\right]^{i+1}} \\ & \times \int_0^{\infty} \int_0^{D(v)} \left[1 - \exp\left(-\frac{E(v,x)}{\Omega_{\mathrm{SI}}}\right)\right] v^j x^i \exp\left[-\left(\frac{v}{2{\sigma_1}^2(\Omega_1, K_1)} + \frac{x}{2{\sigma_2}^2(\Omega_2, K_2)}\right)\right] dx dv - \Bigg\{ \left[1 - \exp\left(-\frac{1}{\Omega_{\mathrm{SI}}\eta\bar{\rho}}\right)\right] \\ & \times \Gamma(j+1) + \frac{1}{\left[2{\sigma_1}^2(\Omega_1, K_1)\right]^{j+1}} \Bigg[\int_0^B v^j \exp\left(-\left(\frac{C(v)}{\Omega_{\mathrm{SI}}} + \frac{v}{2{\sigma_1}^2(\Omega_1, K_1)}\right)\right) dv - \int_{\frac{\gamma_{\mathrm{th}}}{\gamma_{\mathrm{S}}\rho}}^{\infty} \left(1 - \exp\left(-\frac{C(v)}{\Omega_{\mathrm{SI}}}\right)\right) v^j \\ & \times \exp\left(-\frac{v}{2{\sigma_1}^2(\Omega_1, K_1)}\right) dv \Bigg] \Bigg\} \Bigg\{ \frac{\left(\frac{m_2}{K_2}\right)^{m_2}}{\Gamma(m_2)} \sum_{i=0}^{\infty} \frac{\tau_i(K_2, \Delta_2, m_2)}{i!\Gamma(i+1)\left[2{\sigma_1}^2(\Omega_1, K_1)\right]^{j+1}\left[2{\sigma_2}^2(\Omega_2, K_2)\right]^{i+1}} \int_0^{\infty} \int_0^{D(v)} [1 \\ & - \exp\left(-\frac{E(v,x)}{\Omega_{\mathrm{SI}}}\right)] v^j x^i \exp\left[-\left(\frac{v}{2{\sigma_1}^2(\Omega_1, K_1)} + \frac{x}{2{\sigma_2}^2(\Omega_2, K_2)}\right)\right] dx dv + \exp\left(-\frac{1}{\Omega_{\mathrm{SI}}\eta\bar{\rho}}\right) \Bigg\} \Bigg\} + \exp\left(-\frac{1}{\Omega_{\mathrm{SI}}\eta\bar{\rho}}\right) \end{aligned} \tag{30}$$

TABLE 2. Simulation parameters.

Parameter	Value
Number of iterations for simulation	10^7
Path-loss exponent	$\epsilon = 4$
Outage SNR threshold	$\gamma_{\rm th} = 0$ dB
Energy conversion efficiency factor	$\eta = 0.5$
Average channel gain at SI link	$\Omega_{\rm SI} = -10$ dB
Source location	$(0, 0, 0)$
UAV location	$(0.5, 0.24, 0)$
Destination location	$(1, 0, 0)$
Average channel gain	$\Omega_i = d_i^{-\epsilon}$, $i \in \{1, 2\}$
Prob.-of-LOS parameters (urban)	$a = 120$, $b = c = 0$, $d = 24.30$, $e = 1.229$
Prob. of LOS propagation at 1st hop	$P_{1,\rm LOS} = 100\%$
Prob. of LOS propagation at 2nd hop	$P_{2,\rm LOS} = 87.88\%$
FTR parameters for LOS propagation	$K_{\rm LOS} \in \{1, 5\}$ $\Delta_{\rm LOS} = 0$ $m_{\rm LOS} \in \{5, \infty\}$
FTR parameters for NLOS propagation	$K_{\rm NLOS} \to \infty$ $\Delta_{\rm NLOS} = 0$ $m_{\rm NLOS} \in \{1, 5\}$

channel gain $\Omega_{\rm SI}$ at the residual SI link is a dominant factor in determining this outage floor.

V. NUMERICAL RESULTS AND DISCUSSIONS

In this section, we assess six illustrative scenarios and provide Monte Carlo simulations to corroborate our analytical derivations. To this end, we consider a three-dimensional network topology with normalized distances, where the source, the UAV, and the destination are located at the coordinates $(0, 0, 0)$, $(0.5, 0.24, 0)$ and $(1, 0, 0)$, respectively. All distances are normalized with respect to the distance between S and D, $d_{\rm SD}$.[4] We assume that the average channel gain between S and R and between R and D is determined by the path-loss effect, thus being given as $\Omega_i = d_i^{-\epsilon}$, $i \in \{1, 2\}$, respectively, where d_i is the Euclidean distance between the nodes and $\epsilon = 4$ is the path-loss exponent. Additionally, the outage SNR threshold is set to $\gamma_{\rm th} = 0$ dB. Unless otherwise specified, Table 2 summarizes some of the considered simulation parameters for our illustrative scenarios.

Remark 4: Among the potential uses cases for UAV wireless networks, the UAV is envisaged to act as a relay, which connects to a ground base station that provides connectivity to the core network, or as a flying base station, which connects to the core network using a wireless backhaul, so as to provide coverage quickly and cost-effectively. To take full advantage of these setups, the S→R (ground base station-UAV or first hop) link is meant to undergo a LOS condition, whereas the R→D (UAV-destination or second hop) link can be subject to either LOS or NLOS conditions. Thus, for illustration, considering the relevance of this practical scenario, in the following the first hop is assumed to be always at a LOS propagation condition, that is $P_{1,\rm LOS} = 100\%$ and, consequently, $P_{1,\rm NLOS} = 0\%$. As a result, the overall system outage probability in (29) can be simplified to[5]

$$P_{\rm out} = P_{2,\rm LOS} P_{\rm out}^{\rm e2e}\big(K_{1,\rm LOS}, \Delta_{1,\rm LOS}, m_{1,\rm LOS}, K_{2,\rm LOS}, \Delta_{2,\rm LOS}, m_{2,\rm LOS}\big) + P_{2,\rm NLOS} P_{\rm out}^{\rm e2e}\big(K_{1,\rm LOS}, \Delta_{1,\rm LOS}, m_{1,\rm LOS}, K_{2,\rm NLOS}, \Delta_{2,\rm NLOS}, m_{2,\rm NLOS}\big). \quad (36)$$

Since the FTR fading model is a generalized statistical model, for the NLOS propagation condition at the second hop, we consider the particular case of Nakagami-*m* fading, by setting the FTR fading parameters to $K_{2,\rm NLOS} \to \infty$ and $\Delta_{2,\rm NLOS} = 0$, while considering arbitrary values of $m_{2,\rm NLOS}$ [19, Table I]. On the other hand, for the LOS propagation condition at the ith hop, $i \in \{1, 2\}$, we consider two particular cases of the FTR fading model: (*i*) Rician shadowed fading, by setting $\Delta_{i,\rm LOS} = 0$, while considering arbitrary values of $K_{i,\rm LOS}$ and $m_{i,\rm LOS}$; and (*ii*) Rician fading, by setting $\Delta_{i,\rm LOS} = 0$ and $m_{i,\rm LOS} \to \infty$, while considering arbitrary values of $K_{i,\rm LOS}$. Also, for illustration, we consider $K_{i,\rm LOS} = K_{\rm LOS}$, $\Delta_{i,\rm LOS} = \Delta_{\rm LOS}$, $m_{i,\rm LOS} = m_{\rm LOS}$, so that hereafter the subscript i is dropped from the notation of the FTR fading parameters. In our illustrative scenarios, the parameters a, b, c, d, and e, corresponding to the probability of LOS propagation between the UAV and destination (second hop), are set according to an urban scenario, as given in Table 1. Therefore, for the normalized maximum UAV flight height considered herein, $h/d_{\rm SD}$=0.24, we have that $P_{2,\rm LOS} = 87.88\%$ and $P_{2,\rm NLOS} = 12.12\%$.

Fig. 3 shows the system outage performance versus transmit SNR $\gamma_{\rm S}$, for different values of the channel parameters in (36), regarding the LOS and LOS/NLOS propagation conditions at the first hop and second hop, respectively. More specifically, we consider $K_{\rm LOS} \in \{1, 5\}$, $\Delta_{\rm LOS} = 0$, $m_{\rm LOS} = 5$ (Rician shadowed fading) and $K_{\rm LOS} \in \{1, 5\}$, $\Delta_{\rm LOS} = 0$, $m_{\rm LOS} \to \infty$ (Rician fading) as LOS propagation conditions, and $K_{\rm NLOS} \to \infty$, $\Delta_{\rm NLOS} = 0$, $m_{\rm NLOS} \in \{1, 5\}$ (Nakagami-*m* fading) as NLOS propagation conditions. We assume $\alpha = 0.5$ (i.e., equal time allocation between the WPT and SWIPT phases); $\rho = 0.5$ (i.e., equal power splitting between EH and ID at the UAV); $\eta = 0.5$ (energy conversion efficiency); and $\Omega_{\rm SI} = -10$ dB (average channel gain at the residual SI link). Note from this figure how our approximate expression derived in (30) shows a good fit to the simulation results along the entire SNR region, and how our simple asymptotic expression provided in (35) is in perfect agreement with the exact performance at high SNR, as expected. Notably, note that all curves saturate at the same outage floor in the high-SNR regime, irrespective of the channel conditions at the first hop and second hop. Thus, the system performance is chiefly governed by the effect of the residual SI at high SNR, as pointed out previously in Remark 3. We can also notice that, before

4. Herein we consider a practical scenario in which the distance between S and D is 500 m and the maximum flight height of the UAV is 120 m from the ground, according to the European Union Aviation Safety Agency regulation [38].

5. For the computation of the approximate expression of $P_{\rm out}^{\rm e2e}(\cdot, \ldots, \cdot)$ in (30), we have considered up to 40 terms for the summation over both i and j and up to 5 terms for the summation over n, regarding the evaluation of the FTR-fading PDF given as in (5).

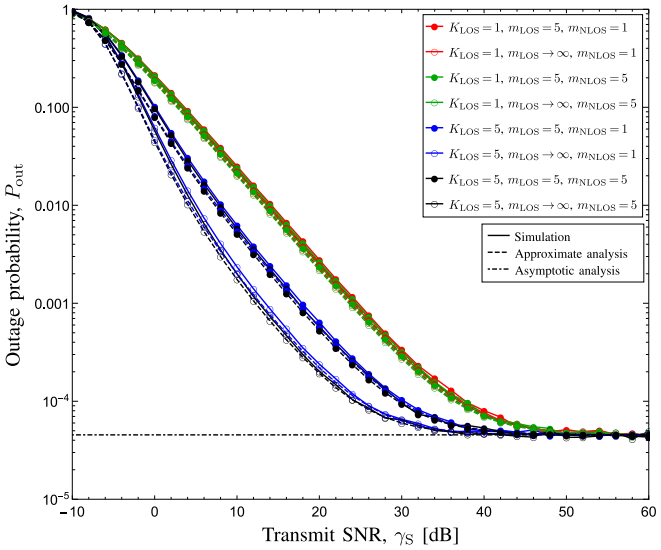

FIGURE 3. Outage probability vs. transmit SNR γ_{S}, with $\Omega_{\text{SI}} = -10$ dB, $\eta = 0.5$, $\alpha = 0.5$, $\rho = 0.5$, and $h/d_{\text{SD}} = 0.24$ ($P_{2,\text{LOS}} = 87.88\%$, $P_{2,\text{NLOS}} = 12.12\%$), considering various FTR fading scenarios: $K_{\text{LOS}} \in \{1, 5\}$, $\Delta_{\text{LOS}} = 0$, $m_{\text{LOS}} = 5$ (Rician shadowed fading) and $K_{\text{LOS}} \in \{1, 5\}$, $\Delta_{\text{LOS}} = 0$, $m_{\text{LOS}} \to \infty$ (Rician fading) for LOS propagation conditions, and $K_{\text{NLOS}} \to \infty$, $\Delta_{\text{NLOS}} = 0$, $m_{\text{NLOS}} \in \{1, 5\}$ (Nakagami-m fading) for NLOS propagation conditions.

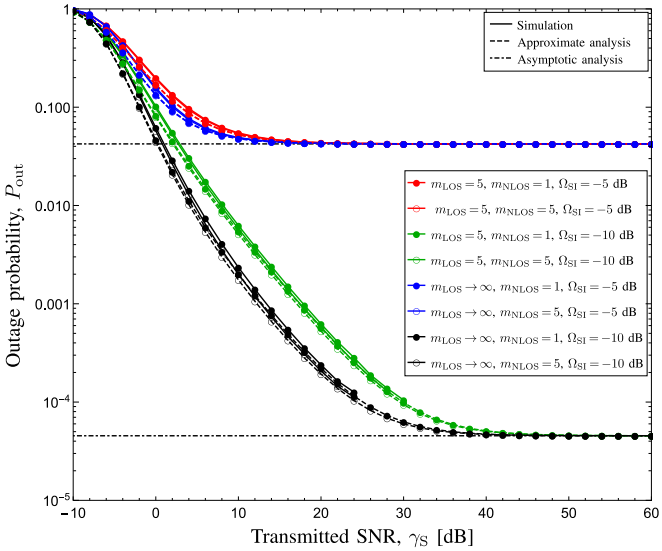

FIGURE 4. Outage probability vs. transmit SNR γ_{S}, for two different values of $\Omega_{\text{SI}} = -5$ and -10 dB, with $\eta = 0.5$, $\alpha = 0.5$, $\rho = 0.5$, and $h/d_{\text{SD}} = 0.24$ ($P_{2,\text{LOS}} = 87.88\%$, $P_{2,\text{NLOS}} = 12.12\%$), considering various FTR fading scenarios: $K_{\text{LOS}} = 5$, $\Delta_{\text{LOS}} = 0$, $m_{\text{LOS}} = 5$ (Rician shadowed fading) and $K_{\text{LOS}} = 5$, $\Delta_{\text{LOS}} = 0$, $m_{\text{LOS}} \to \infty$ (Rician fading) for LOS propagation conditions, and $K_{\text{NLOS}} \to \infty$, $\Delta_{\text{NLOS}} = 0$, $m_{\text{NLOS}} \in \{1, 5\}$ (Nakagami-m fading) for NLOS propagation conditions.

achieving the outage floor, the impact of the K_{LOS} parameter on the system performance prevails over the other fading channel parameters. Indeed, the system shows a significant performance improvement as K_{LOS} increases from 1 to 5. Also, for high values of K_{LOS}, a system performance gain is more noticeable with a variation of the m_{LOS} parameter, when compared to a variation of m_{NLOS}. For example, we can observe that, for the scenarios with a stronger LOS component ($K_{\text{LOS}} = 5$), higher performance gains are achieved for the scenarios with $m_{\text{LOS}} \to \infty$ (i.e., Rician fading), when compared to the cases in which $m_{\text{LOS}} = 5$ (i.e., Rician shadowed fading), whereas the system performance slightly improves with an increase of m_{NLOS} from 1 to 5.

Fig. 4 illustrates the effect of the residual SI inherent to the FD UAV operation on the system outage performance, by considering two distinct values of average channel gain values at the SI link, $\Omega_{\text{SI}} = -5$ and -10 dB, for different fading scenarios, as follows: $K_{\text{LOS}} = 5$, $\Delta_{\text{LOS}} = 0$, $m_{\text{LOS}} = 5$ (Rician shadowed fading) and $K_{\text{LOS}} = 5$, $\Delta_{\text{LOS}} = 0$, $m_{\text{LOS}} \to \infty$ (Rician fading) for LOS propagation conditions, and $K_{\text{NLOS}} \to \infty$, $\Delta_{\text{NLOS}} = 0$, $m_{\text{NLOS}} \in \{1, 5\}$ (Nakagami-m fading) for NLOS propagation conditions. The other system parameters are set to $\eta = 0.5$, $\rho = 0.5$, and $\alpha = 0.5$. We can observe that, similarly as in Fig. 3, regardless of the channel conditions at the first hop and second hop, the system performance converges to outage floor levels ruled by the effect of the residual SI. Note that a decrease in the average channel gain at the SI link from $\Omega_{\text{SI}} = -5$ to -10 dB (i.e., a higher attenuation of residual SI) leads to a significant performance improvement. Note also that the outage floor is attained at higher values of transmit SNR as Ω_{SI} decreases (e.g., $\gamma_{\text{S}} \approx 40$ dB for $\Omega_{\text{SI}} = -10$ dB whereas $\gamma_{\text{S}} \approx 15$ dB for $\Omega_{\text{SI}} = -5$ dB). Moreover, for

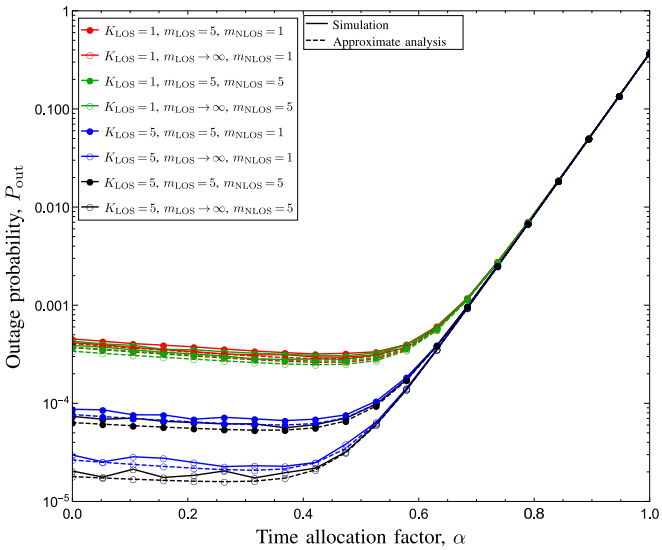

FIGURE 5. Outage probability vs. time allocation factor α, with $\gamma_{\text{S}} = 30$ dB, $\Omega_{\text{SI}} = -10$ dB, $\eta = 0.5$, $\rho = 0.5$, and $h/d_{\text{SD}} = 0.24$ ($P_{2,\text{LOS}} = 87.88\%$, $P_{2,\text{NLOS}} = 12.12\%$), considering various FTR fading scenarios: $K_{\text{LOS}} \in \{1, 5\}$, $\Delta_{\text{LOS}} = 0$, $m_{\text{LOS}} = 5$ (Rician shadowed fading) and $K_{\text{LOS}} \in \{1, 5\}$, $\Delta_{\text{LOS}} = 0$, $m_{\text{LOS}} \to \infty$ (Rician fading) for LOS propagation conditions, and $K_{\text{NLOS}} \to \infty$, $\Delta_{\text{NLOS}} = 0$, $m_{\text{NLOS}} \in \{1, 5\}$ (Nakagami-m fading) for NLOS propagation conditions.

lower levels of residual SI (e.g., $\Omega_{\text{SI}} = -10$ dB), the effect of the FTR fading channel parameter m_{LOS} is more noticeable, when compared to that with higher levels of residual SI ($\Omega_{\text{SI}} = -5$ dB). More specifically, we can observe a higher performance improvement as m_{LOS} increases from 5 to ∞ for $\Omega_{\text{SI}} = -10$ dB, with respect to the performance improvement for $\Omega_{\text{SI}} = -5$ dB.

In Fig. 5, the system outage probability versus the time allocation factor α between the WPT and SWIPT phases is presented, considering the same FTR-fading-parameter

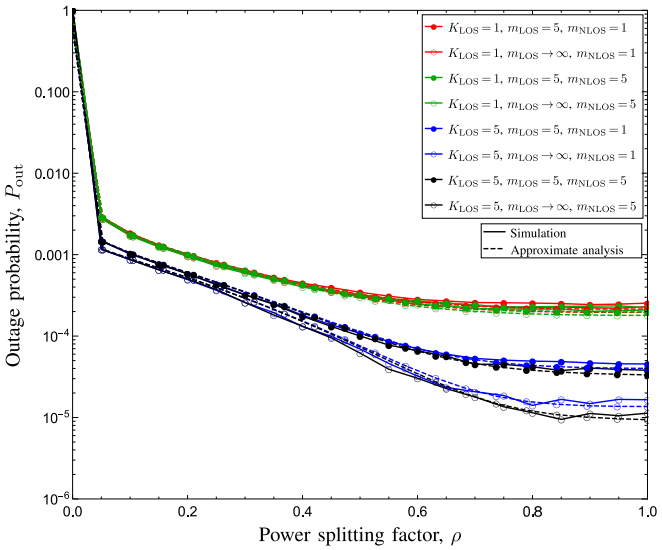

FIGURE 6. Outage probability vs. power splitting factor ρ, with $\gamma_{\text{S}} = 30$ dB, $\Omega_{\text{SI}} = -10$ dB, $\eta = 0.5$, $\alpha = 0.5$, and $h/d_{\text{SD}} = 0.24$ ($P_{2,\text{LOS}} = 87.88\%$, $P_{2,\text{NLOS}} = 12.12\%$), considering various FTR fading scenarios: $K_{\text{LOS}} \in \{1, 5\}$, $\Delta_{\text{LOS}} = 0$, $m_{\text{LOS}} = 5$ (Rician shadowed fading) and $K_{\text{LOS}} \in \{1, 5\}$, $\Delta_{\text{LOS}} = 0$, $m_{\text{LOS}} \to \infty$ (Rician fading) for LOS propagation conditions, and $K_{\text{NLOS}} \to \infty$, $\Delta_{\text{NLOS}} = 0$, $m_{\text{NLOS}} \in \{1, 5\}$ (Nakagami-m fading) for NLOS propagation conditions.

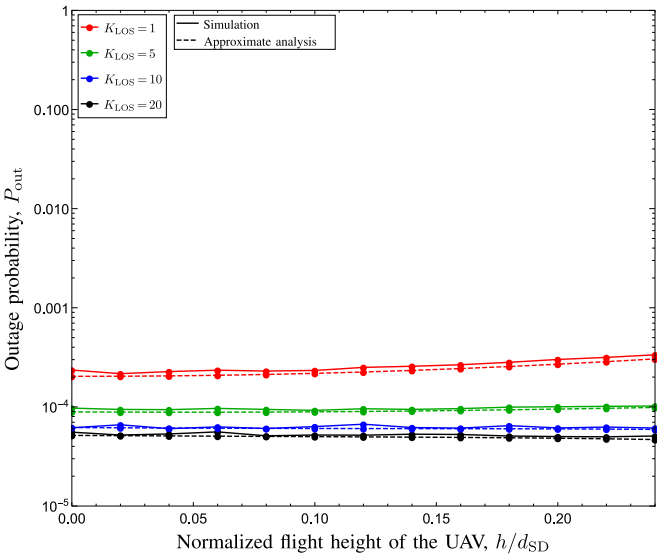

FIGURE 7. Outage probability vs. normalized flight height of the UAV, $h\,/\,d_{\text{SD}}$, with $\gamma_{\text{S}} = 30$ dB, $\Omega_{\text{SI}} = -10$ dB, $\eta = 0.5$, $\alpha = 0.5$, and $\rho = 0.5$, considering various FTR fading scenarios: $K_{\text{LOS}} \in \{1, 5, 10, 20\}$, $\Delta_{\text{LOS}} = 0$, $m_{\text{LOS}} = 5$ (Rician shadowed fading) for LOS propagation conditions, and $K_{\text{NLOS}} \to \infty$, $\Delta_{\text{NLOS}} = 0$, $m_{\text{NLOS}} = 1$ (Rayleigh fading) for NLOS propagation conditions.

configurations as in Fig. 3. We set $\gamma_{\text{S}} = 30$ dB, $\Omega_{\text{SI}} = -10$ dB, $\eta = 0.5$, and $\rho = 0.5$. We can observe that, for values of $\alpha > 0.7$, the system performance deteriorates considerably, regardless of the channel conditions (FTR fading parameters) at the first hop and second hop. This can be explained by the fact that, in this case, most of the time in the communication process is allocated to the WPT phase for energizing the UAV from S, so that the transmit power available at the UAV is higher (vide eq. (15)). As a consequence, the UAV suffers from higher levels of residual SI in the SWIPT phase, thereby degrading the system performance. On the other hand, for values of $\alpha < 0.7$, the effect of the residual SI diminishes and the impact of the channel conditions at the first and second hop can be noticed. In this case, the system performance is consistent with that observed in Fig. 3. That is, a considerable performance improvement is attained with an increase of K_{LOS} from 1 to 5, and the system performance gains are more noticeable with the variation of the fading parameters m_{LOS} and m_{NLOS}, for higher values of K_{LOS}.

Fig. 6 shows the system outage probability versus the power splitting factor ρ in the SWIPT phase, considering the same FTR-fading-parameter configurations as in Fig. 3. Here we set $\gamma_{\text{S}} = 30$ dB, $\Omega_{\text{SI}} = -10$ dB, $\eta = 0.5$, and $\alpha = 0.5$. It can be observed that, for $\rho \approx 0$, the system performance is severely degraded, irrespective of the channel conditions at the first hop and second hop. In this case, as well as for lower values of ρ, since most of the received power at the UAV in the SWIPT phase from S and from the SI link is used for EH, the transmit power available at the UAV is higher, thus aggravating the impact of the residual SI over the system performance. For higher values of ρ, the effect of the residual SI diminishes, so we can notice a system performance behavior consistent with that described in the scenarios of Figs. 3 and 5, regarding the impact of the channel conditions at the first hop and second hop.

Fig. 7 illustrates the system outage probability versus the normalized flight height of the UAV, $h\,/\,d_{\text{SD}}$, considering the following FTR fading scenarios: $K_{\text{LOS}} \in \{1, 5, 10, 20\}$, $\Delta_{\text{LOS}} = 0$, $m_{\text{LOS}} = 5$ (Rician shadowed fading) as LOS propagation conditions, and $K_{\text{NLOS}} \to \infty$, $\Delta_{\text{NLOS}} = 0$, $m_{\text{NLOS}} = 1$ (Rayleigh fading [19, Table I]) as NLOS propagation condition. We assume $\gamma_{\text{S}} = 30$ dB, $\Omega_{\text{SI}} = -10$ dB, $\eta = 0.5$, $\alpha = 0.5$, and $\rho = 0.5$. Note that the system performance improves as K_{LOS} increases, as expected, since the LOS components at the first hop and second hop become stronger. Interestingly, note that the system performance remains roughly the same as the normalized flight height of the UAV increases. This can be explained by the fact that, on the one hand, $P_{2,\text{LOS}}$ given as in (11) is higher as the normalized flight height increases, but on the other hand, the effect of path loss also increases with the distance between the UAV and the ground nodes.

Fig. 8, shown on the next page, illustrates the system outage probability versus the normalized flight height of the UAV, h/d_{SD}, for different values of Δ_{LOS} in the following FTR fading scenarios: $K_{\text{LOS}} = 5$, $\Delta_{\text{LOS}} \in \{0, 0.1, 0.3, 0.5, 0.7, 0.9, 1\}$, $m_{\text{LOS}} = 5$ as LOS propagation conditions, and $K_{\text{NLOS}} \to \infty$, $\Delta_{\text{NLOS}} = 0$, $m_{\text{NLOS}} = 1$ (Rayleigh fading) as NLOS propagation condition. Here we assume $\gamma_{\text{S}} = 30$ dB, $\Omega_{\text{SI}} = -10$ dB, $\eta = 0.5$, $\alpha = 0.5$, and $\rho = 0.5$. Note that the system performance diminishes as Δ_{LOS} increases. The reason for this is as follows. According to the FTR fading model, the magnitudes of the two specular

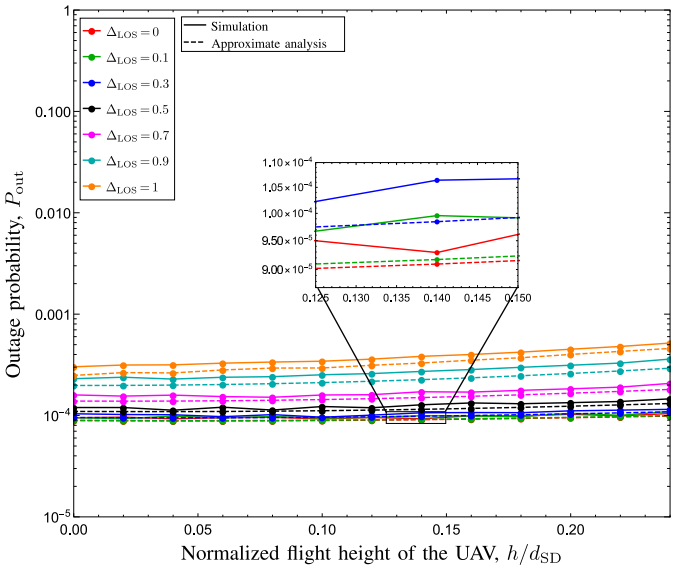

FIGURE 8. Outage probability vs. normalized flight height of the UAV, h / d_{SD}, with $\gamma_S = 30$ dB, $\Omega_{SI} = -10$ dB, $\eta = 0.5$, $\alpha = 0.5$, and $\rho = 0.5$, considering various FTR fading scenarios: $K_{LOS} = 5$, $\Delta_{LOS} \in \{0, 0.1, 0.3, 0.5, 0.7, 0.9, 1\}$, $m_{LOS} = 5$ for LOS propagation conditions, and $K_{NLOS} \to \infty$, $\Delta_{NLOS} = 0$, $m_{NLOS} = 1$ (Rayleigh fading) for NLOS propagation conditions.

components become similar as Δ_{LOS} increases—such magnitudes are equal for $\Delta_{LOS} = 1$, whereas one of the magnitudes is nil for $\Delta_{LOS} = 0$. Moreover, we can notice from (2) that the effect of the specular components prevails over that of the diffuse component for high values of K_{LOS} (we set $K_{LOS} = 5$). Furthermore, the fluctuation of the specular components is mitigated as m_{LOS} increases [19] (we set $m_{LOS} = 5$). This way, the channel undergoes a similar effect to that of the traditional two-ray propagation model (in which only two magnitude-constant specular components are considered, with no diffuse component) for a large enough distance between the transmitter and receiver, so that the (direct and reflected) specular waves have similar magnitudes and combine destructively [39]. On the other hand, for lower values of Δ_{LOS}, the system outage performance improves as the magnitudes of the specular components become dissimilar, so that one specular component is dominant over the other, thus mitigating the destructive combination effect. Also, as observed in Fig. 7, the system performance roughly remains the same as the normalized flight height of the UAV increases, since the higher the flight height of the UAV, the higher are both the probability of LOS condition at the second hop and the path loss at the UAV-ground nodes links.

VI. CONCLUSION

In this paper, the outage performance of a wireless-powered FD-AF UAV relay network operating over FTR fading channels was analyzed. We obtained analytical expressions for the outage probability based on approximate and asymptotic approaches. In particular, our closed-form asymptotic result showed that the FTR fading parameters corresponding to the first hop and second hop play no role on the system outage performance at high SNR. In this case, it was shown to be chiefly governed by the effect of the residual SI, which leads to outage floors, as corroborated by simulation results. In general, it was found that the impact of the K_{LOS} parameter on the system performance prevails over the other fading channel parameters, resulting in a significant system performance improvement as K_{LOS} increases. Also, for high values of K_{LOS} (corresponding to strong-specular-component scenarios), the system performance gain due to an increase in the m_{LOS} parameter is more noticeable. Additionally, it was observed that, for high values of K_{LOS} and m_{LOS}, the outage performance diminishes as Δ_{LOS} decreases, since the specular components combine destructively, more frequently. It was also found that the system outage performance remains roughly the same as the normalized flight height of the UAV increases, since both the probability of LOS condition at the second hop and the path loss at the UAV-ground nodes links increase.

APPENDIX A
PROOF OF PROPOSITION 1

A system outage occurs when the instantaneous received end-to-end SINR, γ_{e2e}, is below a certain threshold γ_{th}. Thus, the outage probability for the considered dual-hop wireless-powered FD UAV relay system can be expressed from (28) as

$$\begin{aligned} P_{out}^{e2e} &= \Pr(\gamma_{e2e} < \gamma_{th}) \\ &= \Pr\left(\frac{\frac{XY}{U+1}}{\frac{X}{U+1} + Y + 1} < \gamma_{th} \right). \end{aligned} \tag{37}$$

Let us denote $A = X/(U+1)$. Then, we use the well-known upper bound for the harmonic mean in (28), whereby we have that $\min\{A, Y\} \geq AY/(A+Y+1)$. It is noteworthy that this upper bound also yields an excellent approximation, especially at high SNR. Thus, the outage probability can be expressed as

$$\begin{aligned} P_{out}^{e2e} &\approx \Pr(\min\{A, Y\} < \gamma_{th}) \\ &\overset{(a)}{=} \Pr(A < \gamma_{th}) + \Pr(Y < \gamma_{th}) \\ &\quad - \Pr(A < \gamma_{th}) \Pr(Y < \gamma_{th}) \\ &= F_A(\gamma_{th}) + F_Y(\gamma_{th}) - F_A(\gamma_{th}) F_Y(\gamma_{th}), \end{aligned} \tag{38}$$

where in step (a) we have developed the $\min\{\cdot,\cdot\}$ function in terms of the marginal probabilities [40, eq. (6.81)]. Next, we determine the marginal CDFs of A and Y. For the former, $F_A(\cdot)$ can be obtained as

$$\begin{aligned} F_A(\gamma_{th}) &= \Pr\left[\frac{X}{U+1} < \gamma_{th} \right] \\ &= \Pr\left[\frac{\rho \gamma_S g_1}{\rho \beta(g_1, g_{SI}) g_{SI} + 1} < \gamma_{th} \right], \end{aligned} \tag{39}$$

where we have used the definitions of X and U given in (25) and (27), respectively. The integration region R_1 for the

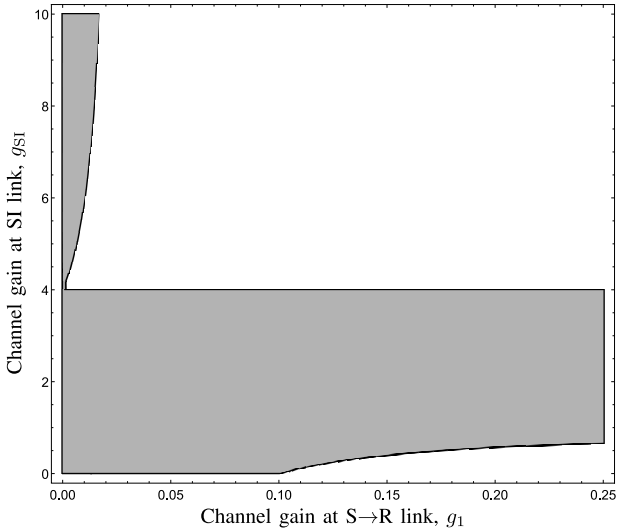

FIGURE 9. Integration region R_1 for the outage event in the argument of Pr(·) in (39), corresponding to the CDF of A, $F_A(\cdot)$.

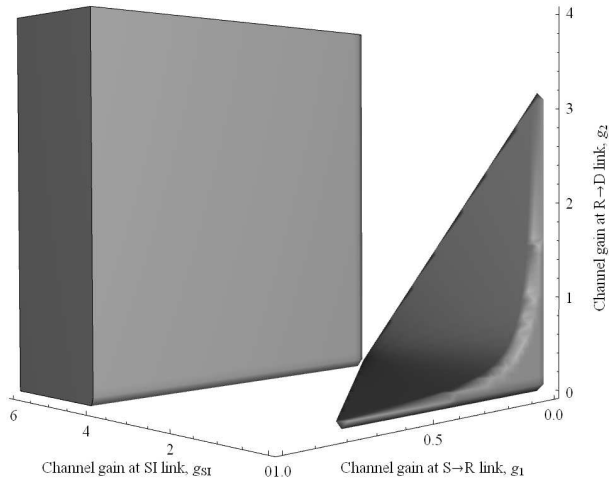

FIGURE 10. Integration region R_2 for the outage event in the argument of Pr(·) in (43), corresponding to the CDF of Y, $F_Y(\cdot)$.

outage event in the argument of Pr(·) in (39) is illustrated in Fig. 9, so that it can be determined as

$$R_1 = \left[0 < g_1 < B \bigcap \left(0 < g_{\rm SI} < \frac{1}{\eta\bar{\rho}} \bigcup g_{\rm SI} > C(g_1)\right)\right] \bigcup \left[B \le g_1 \le \frac{\gamma_{\rm th}}{\gamma_{\rm S}\rho} \bigcap 0 < g_{\rm SI} < \frac{1}{\eta\bar{\rho}}\right] \bigcup \left[g_1 > \frac{\gamma_{\rm th}}{\gamma_{\rm S}\rho} \bigcap C(g_1) < g_{\rm SI} < \frac{1}{\eta\bar{\rho}}\right], \quad (40)$$

where B and $C(\cdot)$ are defined in Proposition 1 as (31) and (32), respectively. Thus, by integrating the PDFs of g_1 and $g_{\rm SI}$ over the region R_1, the CDF of A is obtained as

$$\begin{aligned} F_A(\gamma_{\rm th}) &= \int_0^B f_{g_1}(v)dv \int_0^{\frac{1}{\eta\bar{\rho}}} f_{g_{\rm SI}}(w)dw + \int_0^B \int_{C(v)}^{\infty} f_{g_1}(v) \\ &\quad \times f_{g_{\rm SI}}(w)dwdv + \int_B^{\frac{\gamma_{\rm th}}{\gamma_{\rm S}\rho}} f_{g_1}(v)dv \int_0^{\frac{1}{\eta\bar{\rho}}} f_{g_{\rm SI}}(w)dw \\ &\quad + \int_{\frac{\gamma_{\rm th}}{\gamma_{\rm S}\rho}}^{\infty} \int_{C(v))}^{\frac{1}{\eta\bar{\rho}}} f_{g_1}(v) f_{g_{\rm SI}}(w)dwdv \\ &\overset{(b)}{=} \underbrace{F_{g_1}(B)F_{g_{\rm SI}}\left(\frac{1}{\eta\bar{\rho}}\right)}_{\rm A1} + \underbrace{\int_0^B \left[1 - F_{g_{\rm SI}}(C(v))\right] f_{g_1}(v)dv}_{\rm A2} \\ &\quad + \underbrace{F_{g_{\rm SI}}\left(\frac{1}{\eta\bar{\rho}}\right)\left[F_{g_1}\left(\frac{\gamma_{\rm th}}{\gamma_{\rm S}\rho}\right) - F_{g_1}(B)\right]}_{\rm A3} \\ &\quad + \int_{\frac{\gamma_{\rm th}}{\gamma_{\rm S}\rho}}^{\infty} F_{g_{\rm SI}}\left(\frac{1}{\eta\bar{\rho}}\right) f_{g_1}(v)dv - \int_{\frac{\gamma_{\rm th}}{\gamma_{\rm S}\rho}}^{\infty} F_{g_{\rm SI}}(C(v)) \\ &\quad \times f_{g_1}(v)dv, \end{aligned} \quad (41)$$

where in step (b) we have used distribution function properties. Now, by substituting the expressions of the PDF and CDF of g_1, given as in (5) and (6), and the CDF of $g_{\rm SI}$, given as in (9), into (41), after some mathematical manipulations, we have

$$\begin{aligned} F_A(\gamma_{\rm th}) &= \frac{\left(\frac{m_1}{K_1}\right)^{m_1}}{\Gamma(m_1)} \sum_{j=0}^{\infty} \frac{\tau_j(K_1, \Delta_1, m_1)}{j!\Gamma(j+1)} \\ &\quad \times \left\{\left[1 - \exp\left(-\frac{1}{\Omega_{\rm SI}\eta\bar{\rho}}\right)\right] \times \Gamma(j+1) + \frac{1}{\left[2{\sigma_1}^2(\Omega_1, K_1)\right]^{j+1}} \right. \\ &\quad \times \left[\int_0^B v^j \times \exp\left(-\left(\frac{C(v)}{\Omega_{\rm SI}} + \frac{v}{2{\sigma_1}^2(\Omega_1, K_1)}\right)\right)dv \right. \\ &\quad - \int_{\frac{\gamma_{\rm th}}{\gamma_{\rm S}\rho}}^{\infty} \left(1 - \exp\left(-\frac{C(v)}{\Omega_{\rm SI}}\right)\right) v^j \\ &\quad \left.\left. \times \exp\left(-\frac{v}{2{\sigma_1}^2(\Omega_1, K_1)}\right)dv\right]\right\}. \end{aligned} \quad (42)$$

On the other hand, $F_Y(\gamma_{\rm th})$ can be derived from (26) as

$$\begin{aligned} F_Y(\gamma_{\rm th}) &= \Pr\left[Y < \gamma_{\rm th}\right] \\ &= \Pr\left[\beta(g_1, g_{\rm SI})g_2 < \gamma_{\rm th}\right], \end{aligned} \quad (43)$$

where the integration region R_2 for the outage event in (43) is depicted in Fig. 10, so that it can be expressed as

$$R_2 = g_1 > 0 \bigcap \left\{\left[0 < g_2 < D(g_1) \bigcap \left(0 < g_{\rm SI} < E(g_1, g_2) \bigcup g_{\rm SI} > \frac{1}{\eta\bar{\rho}}\right)\right] \bigcup \left[g_2 \ge D(g_1) \bigcap g_{\rm SI} > \frac{1}{\eta\bar{\rho}}\right]\right\}, \quad (44)$$

where $D(\cdot)$ and $E(\cdot,\cdot)$ are defined in Proposition 1 as (33) and (34), respectively. By integrating the PDFs of g_1, g_2,

and g_{SI} over the region R_2, the CDF of Y is calculated as

$$\begin{aligned} F_Y(\gamma_{\mathrm{th}}) &= \int_0^{\infty}\int_0^{D(v)}\int_0^{E(v,x)} f_{g_1}(v) f_{g_2}(x) f_{g_{\mathrm{SI}}}(w)\,dw\,dx\,dv \\ &\quad + \int_0^{\infty}\int_0^{D(v)} f_{g_1}(v) f_{g_2}(x)\,dx\,dv \int_{\frac{1}{\eta\bar{\rho}}}^{\infty} f_{g_{\mathrm{SI}}}(w)\,dw \\ &\quad + \int_0^{\infty}\int_{D(v)}^{\infty} f_{g_1}(v) f_{g_2}(x)\,dx\,dv \int_{\frac{1}{\eta\bar{\rho}}}^{\infty} f_{g_{\mathrm{SI}}}(w)\,dw \\ &= \underbrace{\int_0^{\infty}\int_0^{D(v)} F_{g_{\mathrm{SI}}}(E(v,x)) f_{g_1}(v) f_{g_2}(x)\,dx\,dv}_{\mathrm{Y1}} \\ &\quad + \left[1 - F_{g_{\mathrm{SI}}}\left(\frac{1}{\eta\bar{\rho}}\right)\right]. \end{aligned} \tag{45}$$

By replacing the PDFs of g_1 and g_2, given as in (5), with the corresponding fading parameters, and the CDF of g_{SI}, given as in (9), into (45), after some mathematical manipulations, we obtain

$$\begin{aligned} F_Y(\gamma_{\mathrm{th}}) &= \frac{\left(\frac{m_1}{K_1}\right)^{m_1}\left(\frac{m_2}{K_2}\right)^{m_2}}{\Gamma(m_1)\Gamma(m_2)} \sum_{j=0}^{\infty}\sum_{i=0}^{\infty} \frac{\tau_j(K_1,\Delta_1,m_1)}{j!\Gamma(j+1)\left[2\sigma_1{}^2(\Omega_1,K_1)\right]^{j+1}} \\ &\quad \times \frac{\tau_i(K_2,\Delta_2,m_2)}{i!\Gamma(i+1)\left[2\sigma_2{}^2(\Omega_2,K_2)\right]^{i+1}} \\ &\quad \times \int_0^{\infty}\int_0^{D(v)} \left[1 - \exp\left(-\frac{E(v,x)}{\Omega_{\mathrm{SI}}}\right)\right] v^j x^i \\ &\quad \times \exp\left[-\left(\frac{v}{2\sigma_1{}^2(\Omega_1,K_1)} + \frac{x}{2\sigma_2{}^2(\Omega_2,K_2)}\right)\right] dx\,dv \\ &\quad + \exp\left(-\frac{1}{\Omega_{\mathrm{SI}}\eta\bar{\rho}}\right). \end{aligned} \tag{46}$$

Thus, by plugging (42) and (46) into (38), an approximation for the outage probability of the considered dual-hop wireless-powered FD UAV relay system over FTR channels can be attained as in (30).

APPENDIX B
PROOF OF PROPOSITION 2

In this case, we assume the high-SNR regime (i.e., $\gamma_{\mathrm{S}} \to \infty$), whereby higher order terms proportional to $1/\gamma_{\mathrm{S}}$ can be neglected. First, let us analyze $F_A(\cdot)$ obtained in (41). Under the high-SNR condition, we have that $B \to 0$, $\gamma_{\mathrm{th}}/(\gamma_{\mathrm{S}}\rho) \to 0$, and

$$\lim_{\gamma_{\mathrm{S}}\to\infty} F_{g_{\mathrm{SI}}}(C(g_1)) = 1 - \exp\left(-\frac{\bar{\alpha}}{\eta\Omega_{\mathrm{SI}}(\bar{\alpha} + \gamma_{\mathrm{th}} - \bar{\alpha}\rho(1+\gamma_{\mathrm{th}}))}\right). \tag{47}$$

Hence, the terms A1 and A3 in (41) tend to zero, by noting that $\gamma(a,0) = 0$ in the definition of the CDF of g_{SI}, given as in (6). Also, the term A2 is equal to zero, since its integration interval is null. Then, at high SNR, $F_A(\cdot)$ reduces from (41) to

$$\begin{aligned} F_A(\gamma_{\mathrm{th}}) &\simeq F_{g_{\mathrm{SI}}}\left(\frac{1}{\eta\bar{\rho}}\right)\int_0^{\infty} f_{g_1}(v)\,dv \\ &\quad - \left[1 - \exp\left(-\frac{\bar{\alpha}}{\eta\Omega_{\mathrm{SI}}(\bar{\alpha} + \gamma_{\mathrm{th}} - \bar{\alpha}\rho(1+\gamma_{\mathrm{th}}))}\right)\right] \\ &\quad \times \int_0^{\infty} f_{g_1}(v)\,dv \\ &= \exp\left(-\frac{\bar{\alpha}}{\eta\Omega_{\mathrm{SI}}(\bar{\alpha} + \gamma_{\mathrm{th}} - \bar{\alpha}\rho(1+\gamma_{\mathrm{th}}))}\right) \\ &\quad - \exp\left(-\frac{1}{\Omega_{\mathrm{SI}}\eta\bar{\rho}}\right). \end{aligned} \tag{48}$$

Now, we analyze $F_Y(\cdot)$ obtained in (45). At high SNR, we have that $D(v) \to 0$. Thus, the term Y1 equals zero, since its integration interval is null. Therefore, at high SNR, $F_Y(\cdot)$ reduces from (45) to

$$\begin{aligned} F_Y(\gamma_{\mathrm{th}}) &\simeq 1 - F_{g_{\mathrm{SI}}}\left(\frac{1}{\eta\bar{\rho}}\right) \\ &= \exp\left(-\frac{1}{\Omega_{\mathrm{SI}}\eta\bar{\rho}}\right). \end{aligned} \tag{49}$$

By substituting (48) and (49) into (38), a closed-form asymptotic expression for the outage probability of the considered dual-hop wireless-powered FD UAV relay system can be obtained as in (35).

REFERENCES

[1] M. Agiwal, A. Roy, and N. Saxena, "Next generation 5G wireless networks: A comprehensive survey," *IEEE Commun. Surveys Tuts.*, vol. 18, no. 3, pp. 1617–1655, 3rd Quart., 2016.

[2] B. Li, Z. Fei, and Y. Zhang, "UAV communications for 5G and beyond: Recent advances and future trends," *IEEE Internet Things J.*, vol. 6, no. 2, pp. 2241–2263, Apr. 2019.

[3] M. Mozaffari, W. Saad, M. Bennis, Y.-H. Nam, and M. Debbah, "A tutorial on UAVs for wireless networks: Applications, challenges, and open problems," *IEEE Commun. Surveys Tuts.*, vol. 21, no. 3, pp. 2334–2360, 3rd Quart., 2019.

[4] E. E. B. Olivo, D. P. M. Osorio, H. Alves, J. C. S. S. Filho, and M. Latva-Aho, "Cognitive full-duplex decode-and-forward relaying networks with usable direct link and transmit-power constraints," *IEEE Access*, vol. 6, pp. 24983–24995, 2018.

[5] D. P. M. Osorio, E. E. B. Olivo, H. Alves, J. C. S. S. Filho, and M. Latva-Aho, "An adaptive transmission scheme for amplify-and-forward relaying networks," *IEEE Trans. Commun.*, vol. 65, no. 1, pp. 66–78, Jan. 2017.

[6] E. E. B. Olivo, D. P. M. Osorio, H. Alves, J. C. S. S. Filho, and M. Latva-aho, "An adaptive transmission scheme for cognitive decode-and-forward relaying networks: Half duplex, full duplex, or no cooperation," *IEEE Trans. Wireless Commun.*, vol. 15, no. 8, pp. 5586–5602, Aug. 2016.

[7] M. Duarte, C. Dick, and A. Sabharwal, "Experiment-driven characterization of full-duplex wireless systems," *IEEE Trans. Wireless Commun.*, vol. 11, no. 12, pp. 4296–4307, Dec. 2012.

[8] E. Ahmed and A. M. Eltawil, "All-digital self-interference cancellation technique for full-duplex systems," *IEEE Trans. Wireless Commun.*, vol. 14, no. 7, pp. 3519–3532, Jul. 2015.

[9] D. Korpi, M. Heino, C. Icheln, K. Haneda, and M. Valkama, "Compact inband full-duplex relays with beyond 100 dB self-interference suppression: Enabling techniques and field measurements," *IEEE Trans. Antennas Propag.*, vol. 65, no. 2, pp. 960–965, Feb. 2017.

[10] J. Huang, C.-C. Xing, and C. Wang, "Simultaneous wireless information and power transfer: Technologies, applications, and research challenges," *IEEE Commun. Mag.*, vol. 55, no. 11, pp. 26–32, Nov. 2017.

[11] E. N. Egashira, E. E. B. Olivo, D. P. M. Osorio, and H. Alves, "Secrecy performance of untrustworthy AF relay networks using cooperative jamming and SWIPT," in *Proc. PIMRC*, Istanbul, Turkey, Sep. 2019, pp. 1–6.

[12] I. Krikidis, S. Timotheou, S. Nikolaou, G. Zheng, D. W. K. Ng, and R. Schober, "Simultaneous wireless information and power transfer in modern communication systems," *IEEE Commun. Mag.*, vol. 52, no. 11, pp. 104–110, Nov. 2014.

[13] X. Xie, J. Chen, and Y. Fu, "Outage performance and QoS optimization in full-duplex system with non-linear energy harvesting model," *IEEE Access*, vol. 6, pp. 44281–44290, 2018.
[14] K. Xu *et al.*, "Beam-domain SWIPT for mMIMO system with nonlinear energy harvesting legitimate terminals and a non-cooperative terminal," *IEEE Trans. Green Commun. Netw*, vol. 3, no. 3, pp. 703–720, Sep. 2019.
[15] C. Zhong, H. A. Suraweera, G. Zheng, I. Krikidis, and Z. Zhang, "Wireless information and power transfer with full duplex relaying," *IEEE Trans. Commun.*, vol. 62, no. 10, pp. 3447–3461, Oct. 2014.
[16] M. Mohammadi, B. K. Chalise, H. A. Suraweera, G. Zheng, and I. Krikidis, "Throughput analysis and optimization of wireless-powered multiple antenna full-duplex relay systems," *IEEE Trans. Commun*, vol. 64, no. 4, pp. 1769–1785, Apr. 2016.
[17] K. Xu, Z. Shen, Y. Wang, X. Xia, and D. Zhang, "Hybrid time-switching and power splitting SWIPT for full-duplex massive MIMO systems: A beam-domain approach," *IEEE Trans. Veh. Technol.*, vol. 67, no. 8, pp. 7257–7274, Aug. 2018.
[18] Z. Xiao, P. Xia, and X.-G. Xia, "Enabling UAV cellular with millimeter-wave communication: Potentials and approaches," *IEEE Commun. Mag.*, vol. 54, no. 5, pp. 66–73, May 2016.
[19] J. M. Romero-Jerez, F. J. Lopez-Martinez, J. F. Paris, and A. J. Goldsmith, "The fluctuating two-ray fading model: Statistical characterization and performance analysis," *IEEE Trans. Wireless Commun.*, vol. 16, no. 7, pp. 4420–4432, Jul. 2017.
[20] M. K. Samimi, G. R. MacCartney, S. Sun, and T. S. Rappaport, "28 GHz millimeter-wave ultrawideband small-scale fading models in wireless channels," *Proc. IEEE 83rd Veh. Technol. Conf.*, Nanjing, China, May 2016, pp. 1–6.
[21] J. Zheng, J. Zhang, S. Chen, H. Zhao, and B. Ai, "Wireless powered UAV relay communications over fluctuating two-ray fading channels," *Phys. Commun.*, vol. 35, Aug. 2019, Art. no. 100724.
[22] T. Z. H. Ernest, A. S. Madhukumar, R. P. Sirigina, and A. K. Krishna, "A power series approach for hybrid-duplex UAV communication systems under Rician shadowed fading," *IEEE Access*, vol. 7, pp. 76949–76966, 2019.
[23] L. Yang, J. Chen, M. O. Hasna, and H.-C. Yang, "Outage performance of UAV-assisted relaying systems with RF energy harvesting," *IEEE Commun. Lett.*, vol. 22, no. 12, pp. 2471–2474, Dec. 2018.
[24] S. Yin, Y. Zhao, L. Li, and F. R. Yu, "UAV-assisted cooperative communications with power-splitting information and power transfer," *IEEE Trans. Green Commun. Netw.*, vol. 3, no. 4, pp. 1044–1057, Dec. 2019.
[25] D. N. K. Jayakody, T. D. P. Perera, A. Ghrayeb, and M. O. Hasna, "Self-energized UAV-assisted scheme for cooperative wireless relay networks," *IEEE Trans. Veh. Technol.*, vol. 69, no. 1, pp. 578–592, Jan. 2020.
[26] B. Ji, Y. Li, D. Cao, C. Li, S. Mumtaz, and D. Wang, "Secrecy performance analysis of UAV assisted relay transmission for cognitive network with energy harvesting," *IEEE Trans. Veh. Technol.*, vol. 69, no. 7, pp. 7404–7415, Jul. 2020.
[27] N. P. Le *et al.*, "Energy-harvesting aided unmanned aerial vehicles for reliable ground user localization and communications under Lognormal-Nakagami-*m* fading channels," *IEEE Trans. Veh. Technol.*, vol. 70, no. 2, pp. 1632–1647, Feb. 2021.
[28] L. Zhu, J. Zhang, Z. Xiao, X. Cao, X.-G. Xia, and R. Schober, "Millimeter-wave full-duplex UAV relay: Joint positioning, beamforming, and power control," *IEEE J. Sel. Areas Commun*, vol. 38, no. 9, pp. 2057–2073, Sep. 2020.
[29] B. Li, S. Zhao, R. Zhang, and L. Yang, "Full-duplex UAV relaying for multiple user pairs," *IEEE Internet Things J.*, vol. 8, no. 6, pp. 4657–4667, Mar. 2021.
[30] A. A. Khuwaja, G. Zheng, Y. Chen, and W. Feng, "Optimum deployment of multiple UAVs for coverage area maximization in the presence of co-channel interference," *IEEE Access*, vol. 7, pp. 85203–85212, 2019.
[31] O. S. Badarneh and D. B. da Costa, "Cascaded fluctuating two-ray fading channels," *IEEE Commun. Lett.*, vol. 23, no. 9, pp. 1497–1500, Sep. 2019.
[32] I. S. Gradshteyn and I. M. Ryzhik, *Table of Integrals, Series, and Products*, 8th ed. San Diego, CA, USA: Academic, 2015.
[33] J. Zheng, J. Zhang, G. Pan, J. Cheng, and B. Ai, "Sum of squared fluctuating two-ray random variables with wireless applications," *IEEE Trans. Veh. Technol.*, vol. 68, no. 8, pp. 8173–8177, Aug. 2019.
[34] O. S. Badarneh, D. B. da Costa, M. Benjillali, and M.-S. Alouini, "Ratio of products of fluctuating two-ray variates," *IEEE Commun. Lett.*, vol. 23, no. 11, pp. 1944–1948, Nov. 2019.
[35] J. Zhang, W. Zeng, X. Li, Q. Sun, and K. P. Peppas, "New results on the fluctuating two-ray model with arbitrary fading parameters and its applications," *IEEE Trans. Veh. Technol.*, vol. 67, no. 3, pp. 2766–2770, Mar. 2018.
[36] J. Holis and P. Pechac, "Elevation dependent shadowing model for mobile communications via high altitude platforms in built-up areas," *IEEE Trans. Antennas Propag.*, vol. 56, no. 4, pp. 1078–1084, Apr. 2008.
[37] D. P. M. Osorio, E. E. B. Olivo, H. Alves, J. C. S. S. Filho, and M. Latva-aho, "Exploiting the direct link in full-duplex amplify-and-forward relaying networks," *IEEE Signal Process. Lett.*, vol. 22, no. 10, pp. 1766–1770, Oct. 2015.
[38] European Union Aviation Safety Agency. (2021). *How High Can I Fly My Drone?* [Online]. Available: https://www.easa.europa.eu/
[39] A. Goldsmith, *Wireless Communications*. Cambridge, U.K.: Cambridge Univ. Press, 2005.
[40] A. Papoulis, *Probability, Random Variables, and Stochastic Processes*, 4th ed. New York, NY, USA: McGraw-Hill, 2002.

DANIEL DE PAIVA MUCIN received the B.Sc. degree in telecommunication engineering and the M.Sc degree in electrical engineering from São Paulo State University (UNESP), Campus of São João da Boa Vista, Brazil, in 2018 and 2021, respectively. His research interests are related to wireless communications with emphasis on UAV-based communications, cognitive relaying networks, and full duplex relaying.

DIANA PAMELA MOYA OSORIO (Member, IEEE) was born in Quito, Ecuador. She received the B.Sc. degree in electronics and telecommunications engineering from Armed Forces University (ESPE), Sangolquí, Ecuador, in 2008, and the M.Sc. and D.Sc. degrees in electrical engineering with emphasis on telecommunications and telematics from the University of Campinas, Campinas, Brazil, in 2011 and 2015, respectively. In 2018, she was a Visiting Researcher with the Centre for Wireless Communications (CWC), University of Oulu, Finland. Since 2015, she has been an Assistant Professor with the Department of Electrical Engineering, Federal University of São Carlos (UFSCar), São Carlos, Brazil. In 2020, she joined the 6GFlagship Program with CWC, University of Oulu, as a Senior Research Fellow, where she is also an Adjunct Professor of Physical Layer Techniques for Security. She has been a Postdoctoral Researcher for the Academy of Finland since 2020. Her research interests include wireless communications in general, 5G and 6G networks, and physical layer security. She has served as a TPC and a reviewer for several journals and conferences.

EDGAR EDUARDO BENITEZ OLIVO (Member, IEEE) received the B.Sc. degree in electronics and telecommunications engineering from the Armed Forces University (ESPE), Ecuador, in 2008, and the M.Sc. and D.Sc. degrees in electrical engineering from the University of Campinas, Brazil, in 2011 and 2015, respectively. In 2014, he held a visiting researcher position with the Centre for Wireless Communications, University of Oulu, Finland. Since 2016, he has been with São Paulo State University (UNESP), Campus of São João da Boa Vista, Brazil, as an Assistant Professor. His research interests lie in the area of wireless communications, with a current focus on enabling technologies for B5G/6G networks. He has served as a reviewer for many journals and has been involved as a TPC member and reviewer in several conferences.